Comparative study of six failure criteria via numerical simulation of stamped DP600 steel

Lucas Marcondes Ribas
Federal University of Paraná
Manolo Lutero Gipiela (mgipiela@yahoo.com.br)
Universidade Federal do Parana
Sergio Fernando Lajarin
Federal University of Paraná
Ravilson Antonio Chemin Filho
Federal University of Paraná
Paulo Victor Prestes Marcondes
Federal University of Paraná

Research Article

Keywords: Stamping, Failure Criteria, AHSS, Finite Element Analysis

Posted Date: January 27th, 2022

DOI: https://doi.org/10.21203/rs.3.rs-1252026/v1

Abstract

During the development of an automobile part obtained by stamping process, time and money are required aiming process planning and set up of a new tooling. One of the difficulties in stamping is to know if the chosen material will have sufficient formability to reach the final form required by the project. Because of this difficulty it is very interesting to propose a method that can accurately simulate the forming process. The failure criteria can be mathematical or empirical models capable of determining the onset of necking for each stress/strain states. It is interesting to find a failure criterion that can be easily determined and provides a good ability to detect the failure accurately. In this study six different failure criteria were studied. Five of them are classified as ductile damage models and they depend on the stress triaxiality and plastic strain. The last criteria depend only on the deformations in the main directions and it is called the forming limit curve (FLC). It was used computational models through finite element analysis (FEA). The formability was evaluated by monitoring the displacement of the punch until the failure of the material. Some failure criteria have been able to provide approximation errors in the range of 0.7 - 5% which makes them interesting for practical implementation in the industry.

1. Introduction

The significant increase of advanced high strength steels (AHSS) applications in vehicles was necessary due to the environmental demands that lead to decreased pollutants by reducing vehicle weights and maintaining the mechanical strength levels of materials already used in industry [1]. During the design phase of a product, time and money are spent during the tooling set up [2]. Depending on the geometry of the desired product the selected material can be unable to deform to achieve such requirement. Determining a failure criterion that can accurately describe the fracture mechanism of a metallic materials can be very useful in sheet metal parts development.

Two groups of failure criteria modes that are applied in the stamping process were carried out. The first is the forming limit curve (FLC) and the second is the ductile damage mode criteria. The FLC criteria is usually obtained by Nakazima test based on the two main strains, i. e., width-by-length. On the other hand, the ductile damage criteria are based on the complete state of stresses and strains involved in the stamping process [3]. The fracture starts when the equivalent plastic strain reaches a critical value D_c, Eq. 1.

$$D\left(\bar{\epsilon}_p\right) = \int_0^{\bar{\epsilon}_f} \frac{d\bar{\epsilon}_p}{f(\eta, \bar{\theta})} \quad (1)$$

In the Eq. 1 $\bar{\epsilon}_p$ is the equivalent plastic strain, $\bar{\epsilon}_f$ is the equivalent plastic strain for fracture, $D\left(\bar{\epsilon}_p\right)$ is called the ductile failure criteria or damage factor, which indicates the onset of fracture when it reaches

the critical value D_c = 1, since at the time of fracture the relation $\bar{\epsilon}_p = \bar{\epsilon}_f$ is suggested by [4]. The parameters e $\bar{\theta}$ are called triaxiality or triaxial stress and Lode angle, respectively, both are stress-dependent parameters. This criteria mode uses the graph x $\bar{\epsilon}_f$ to describe the failure limits of a given material and is called the fracture envelope. Mathematical models are determined to obtain an equation that can provide the plastic deformation in the fracture based on the stresses applied to the specimen. Habibi et al. [5] used five mathematical models of the ductile damage model, they are: Modified Mohr Coulomb [6], Maximum Shear Stress [7], Johson-Cook [8], Lou and Huh [9] and Oh *et al.* [10] All these mathematical models are showed below.

Modified Mohr Coulomb (MMC):

$$\bar{\epsilon}_f = \left\{ \frac{A}{C_2} \left[C_3 + \frac{\sqrt{3}}{2-\sqrt{3}} \left(1 - C_3\right) \left(\sqrt{\frac{3+\mu^2}{3}} - 1 \right) \right] X \left[\sqrt{\frac{1+C_1^2}{3+\mu^2}} + C_1 \left(\frac{1}{3} \left(\frac{-\mu}{\sqrt{3+\mu^2}} \right) \right) \right] \right\}^{-\frac{1}{n}}$$

(2)

Maximum Shear Stress (MSS):

$$\bar{\epsilon}_f = \left\{ \frac{A}{C_2\sqrt{3+\mu^2}} \right\}^{-\frac{1}{n}} \quad (3)$$

Johson-Cook:

$$\bar{\epsilon}_f = C_1 + C_2 e^{(-C_3)} \quad (4)$$

Lou e Huh:

$$\bar{\epsilon}_f = C_1 \left(\frac{2}{3\sqrt{3+\mu^2}} \right)^{-C_2} \left(\frac{1+3}{2} \right)^{-C_3} \quad (5)$$

Oh et al.:

$$\bar{\epsilon}_f = C_1 \left\{ + \frac{3-\mu}{3\sqrt{3+\mu^2}} \right\}^{-1} \quad (6)$$

The constants C_1,$C_2$and C_3 are obtained through practical tests [3]. The number of constants in each model indicates the number of tests required to determine the complete mathematical model. The main need for the experiments is to know the exact triaxiality of each test. The variable μ is called the Lode parameter. The triaxiality value is described in Eq. 7.

$$ = -\frac{p}{q} \quad (7)$$

Where,

$$p = -\frac{1}{3}\left(\sigma_1 + \sigma_2 + \sigma_3\right) \quad (8)$$

$$q = \sqrt{\frac{1}{2}\left[\left(\sigma_1 - \sigma_2\right)^2 + \left(\sigma_2 - \sigma_3\right)^2 + \left(\sigma_3 - \sigma_1\right)^2\right]} \quad (9)$$

The term p (Eq. 8) is the hydrostatic pressure and q (Eq. 9) is the Von Mises stress or equivalent stress. Both are expressed in terms of stresses in the principal directions (σ_1, σ_2 e σ_3). For uniaxial tensile test the value of is 0.33 since $\sigma_2 = \sigma_3 = 0$. For pure compression test the value of is -0.33 since the same stress state from tensile test is obtained but σ_1 acting in the opposite direction. For values that simulate another stress state it is necessary to change the specimen geometry to obtain a known triaxial stress state [3,11]. The Fig. 1 shows some specimens used by [3] to plot the curve x $\bar{\epsilon}_f$.

The purpose of the work is to find an initial estimation of formability measured by punch depth which can be implemented by a quick input during the development a new stamping geometry. This initial estimative is obtained by using different failure criteria on FEA simulation instead of practical tests that are usually required to measure forming limits.

2. Materials And Methods

The computational code was developed in a commercial version of ABAQUS software which was fed with data from the DP600 steel. The results of the present work were compared to the results obtained with the experimental data presented in the study [12], where the formability of the DP600 steel with the variation of the blank holder load (BHL) were previously evaluated. To prove the model validity the configurations of the blank, die, BHL and the punch were defined in order to get closer to the parameters used by [12]. The Nakazima tool geometry used in the practical tests and in the computational model are shown in Fig. 2.

The blank holder, die and punch were modelled as solid shell elements since their deformation are not evaluated during the analysis. The sheet was modeled as deformable shell due to purpose of analyze its deformation during the process. The advantage of the shell format is reduced iteration time. The shell element type for the sheet was S4R integration type. The model was divided in three parts. The 1st part

was the contact between blank holder and die, the 2nd part is the blank holder force application and the 3rd part was the vertical motion from the punch pushing the sheet downwards through the die. For this model it was used the penalty contact method.

The failure criteria used in the work are approximated for the plane stress state and this approach is also interesting for the sheet modeling in the shell format. The shell format will not consider the analysis of stress and deformation in the direction of the sheet thickness [13]. Fig. 3 summarizes the formats and types defined for the simulations.

The finite element simulation was done in three steps: 1st step - contact between the blank holder and the blank; 2nd step - application of the BHL load and the 3rd step - vertical displacement of the punch. The default value of the time period in ABAQUS application was 1, i.e., the time varies from 0.0 to 1.0 throughout the simulation step. The time increments in each analysis are simply fractions of the total period of each simulation step [13]. In this study the punch displacement step time is 10x longer than the time of the 1st and 2nd steps. For the computational simulations the same BLF levels used by [12], in his practical tests, were defined for the present study. In this case, three BLF loads were used: 58tf, 80tf and 130tf.

It is important to clarify the conditions under which the failure criteria are reached in the ABAQUS models defined in this work. Abaqus software automatically delete the elements at the crack location. It was selected an increment of 0.1mm from punch displacement to extract the exact punch displacement when the crack initiates.

To define the fracture envelopes of Eq. 2, 3, 4, 5 and 6 it was necessary to leave all terms on the right side of the equation as a function of . This allows to vary the value of with an increment value and observe the corresponding value of $\bar{\epsilon}_f$ for each value of . In this way it is possible to obtain the trace of the fracture envelope curve. According to [2] for the plane strain state the Lode angle can be related to triaxiality through the Eq. 10:

$$-\frac{27}{2}\left(^2-\frac{1}{3}\right)=\text{sen}\left(\frac{\bar{\theta}\pi}{2}\right) \quad (10)$$

The Lode angle and the Lode parameter are related by the Eq. 11.

$$tg\left(\bar{\theta}\right)=\frac{\sqrt{3}(1+\mu)}{3-\mu} \quad (11)$$

Using Eq. 10 and 11 to leave Eq. 2, 3, 4, 5 and 6 in function only of triaxiality we obtain the equations below:

Modified Mohr Coulomb:

$$\bar{\epsilon}_f = \left\{ \frac{A.f_3}{C_2} \left[\sqrt{\frac{1+C_1^2}{3}}.f_1 + C_1 \left(\square + \frac{f_2}{3} \right) \right] \right\}^{-\frac{1}{n}} \quad (12)$$

Maximum Shear Stress:

$$\bar{\epsilon}_f = \left\{ \frac{A.f_1}{C_2\sqrt{3}} \right\}^{-\frac{1}{n}} \quad (13)$$

Johson-Cook:

$$\bar{\epsilon}_f = C_1 + C_2 e^{(-C_3 \square)} \quad (14)$$

Lou e Huh:

$$\bar{\epsilon}_f = C_1 \left(\frac{2\sqrt{3}}{9} f_1 \right)^{-C_2} \left(\frac{1+3\square}{2} \right)^{-C_3} \quad (15)$$

Oh et al.:

$$\bar{\epsilon}_f = C_1 \left(\square + \frac{f_1}{\sqrt{3}} + \frac{f_2}{3} \right)^{-1} \quad (16)$$

The values of f_1, $f_2$and f_3 are called simplifying functions and it can be obtained according to the Eq. 17, 18 and 19 [14].

$$\mathrm{f_1} = \cos\left\{ \frac{1}{3}\mathrm{sen}^{-1} \left[-\frac{27}{2}\square \left(\square^2 - \frac{1}{3} \right) \right] \right\} \quad (17)$$

$$\mathrm{f_2} = \mathrm{sen}\left\{ \frac{1}{3}\mathrm{sen}^{-1} \left[-\frac{27}{2}\square \left(\square^2 - \frac{1}{3} \right) \right] \right\} \quad (18)$$

$$\mathrm{f_3} = \mathrm{C_3} + \frac{\sqrt{3}}{\left(2-\sqrt{3}\right)} \left(1 - \mathrm{C_3}\right) \left(\frac{1}{\mathrm{f_1}} - 1 \right) \quad (19)$$

Using the calibration constants obtained by [1] for the DP600 steel, the five fracture envelopes in Fig. 4 were obtained. The curve data were useful to feed the ABAQUS software as a failure criteria. Usually tests that provides a known stress test are chosen to calculate the constants. Pure tensile test, pure compression or pure shear tests are used for that, Fig. 1.

The shape of the curve from Fig. 4 is explained by the behavior from the ductile damage equation for each criteria. In this case Eq. 14 for Johson-Cook and Eq. 16 for Oh et al. Johson-Cook has an exponential equation while Oh et al. has a linear equation. It was not selected to use criteria with similar curve shapes since Oh et al. per example presented minor errors when compared to other criteria as illustrated by Fig. 7.

The values of ϵ_1 and ϵ_2 (major and minor true strains) were also obtained by [12] via the Nakazima test of DP600. These values were used to implement the FLC criteria in the computational model. The fundamental mechanical properties and true stress-by-true strain curve for DP600 steel obtained by [15] as illustrated in Fig. 5 were also used.

3. Results

The stamping depth was the compared variable among the failure criteria (total punch displacement at the exact fracture point). Fig. 6 demonstrates the exact moment when the fracture occurs in the blank. For the three BHL (58tf, 80tf and 130tf) the errors were calculated in relation to the practical values obtained from the punch force vs displacement curves determined by [12]. Fig. 6 also illustrates a crack initiation in the sheet during the computational model execution considering a failure criteria inserted in the material characterization.

The stamping depths obtained at the crack starting are summarized in Tab. 1.

Table 1: Stamping depths (in mm) obtained in the tests.

Failure criteria	Johson-cook	Lou e Huh	MMC	MSS	Oh et al.	FLD	Chemin Filho (2011)
58tf	45.6	58.5	47.4	45.3	48.3	54	53.6
80tf	42.6	54.6	45.6	43.8	44.7	50.1	48
130tf	39.2	51	42.6	40.8	40.8	46.2	39.6

The computational results for the BHL of 58tf showed very good convergence with the practical results obtained by [12], for the FLC criterion, and with a good convergence for the Lou and Huh criterion, is illustrated in Fig. 7(a).

The magnitude of the errors for this load can be attributed to the different mechanical properties of DP600 steels used by [12], [5] and [11]. The data used to feed the computational model were obtained by [11] and the failure criteria calibration constants were the same used by [5] in practical and computational tests with DP600 steel.

For the BHL of 80tf the criteria that shown nearest results to [12] were the FLC and the Modified Mohr-Coulomb (MMC), as can be seen in the Fig. 7(b).

The errors obtained for the simulation with the BHL of 130tf are shown in Fig. 7(c). The results for Johnson-Cook, Maximum Shear Stress (MSS) and Oh et al. were the ones that came closer to the results obtained by [12].

It was observed that Lou & Huh and the FLC criteria showed larger errors when the sheet restriction is not so expressive. The same meshing was applied for all the simulations and if the mesh is reduced all the results could be changed by the same amount proportionally. It was used a mesh of 0.5x0.5 elements at a circular section of 50mm radius and 2x2 elements at the remaining sheet, Fig. 8.

Most of the maximum punch depth values obtained for the computationally simulated failure criteria showed a linear trend or very close to linear. On the other hand, the results obtained by [12] deviate from the trend obtained from the computational results, see Fig. 9. The computational deviation can be justified by do not consider the changes in the elasticity modulus during the plastic deformation of the sheet; furthermore, lubrication parameters and different deformation rate from those used by [12] can also be attributed to this behavior.

It was observed that some graphic lines did not presented a linear behavior related to forming depth when compared to other lines. The line with the practical results obtained by [12] was the one that did not present a linear behavior and one of the aspects that could explain is that the numeric models made by FEA could not explain some variances in the material that could happen during deformation such as changes in the modulus of elasticity during plastic deformation. Some better approximations can be done by using sub-routines during simulations which could be the focus on futures studies.

The failure criteria obtained by FEA did not achieve a greater results accuracy when compared to the failure criteria obtained by the Nakazima test [12]. For the elaboration of the FLC failure criteria, a sequence of tests with controlled conditions and parameters is required, which makes difficult the obtention of all the data. Some of the failure criteria of the ductile damage model require only one uniaxial tensile test for its determination, which becomes interesting when compared to the FLC criteria.

It was observed that for each blank holder load there was a criteria that was closer to the results obtained by [12], such behavior can be studied for the selection of the rupture criterion to be used in a given or specific application. For example, in addition to the FLC criterion, Lou & Huh criterion obtained a reasonable simulation error for loads of 58tf while the Johson-Cook criterion resulted in a 1% error for 130tf load.

In the cases with a small amount of sheet restriction, an approximation with 6% error was obtained for the Oh et al. criterion when compared to the result reproduced by [12] for blank holder load of 58tf. The FLC criterion distanced itself from the results obtained by [12] in cases with greater sheet restriction, while the MSS criterion raised with the data of [16] resulted in an error of 7.1% for the blank holder load of

130tf. Such errors become interesting since the determination of the Oh et al. and MSS criteria require only one tensile test.

The approximations obtained by the Habibi et al. criteria [5] diverged from the results of [12] due to the fact that the DP600 steel used in the tests to determine the calibration constants did not have the same characteristics (composition and mechanical properties) of the steel used by [12].

In summary, the following factors can be highlighted from the performed experiments:

- Linear behavior of the stamping depths obtained by the computational tests was observed while the same trend was not observed for the experiments performed by [12] - further study of the fracture mechanism of DP or AHSS steels becomes necessary;

- Some criteria showed lower errors at specific blank holder loads, such result can be used for a practical implementation having the sheet restriction intensity as a selection criterion for the rupture criteria;

- Criteria where only one uniaxial tensile test is needed for model calibration, showed errors in the range of 3-7%. This fact becomes interesting when compared to the determination of a failure criterion by Nakazima test or via three practical tests according to some criteria of the ductile damage model.

4. Conclusion

The failure criteria numerically obtained did not reach a good precision in the results if compared to the failure criteria obtained by the FLC plotted with Nakazima test data. In the FLC failure criteria a sequence of tests with controlled conditions and parameters is required and it makes hard to obtain the FLC. Some failure criteria for ductile damage models require only one uniaxial tensile test to be determined becoming interesting when compared to the FLC criterion.

In this study it was observed that for each blank holder load there was a failure criterion that was closer to the results obtained by [12]. Such behavior can be studied for the selection of the failure criteria to be applied in a given application. For example, in addition to the FLC criterion, Lou and Huh criterion showed a reasonable simulation error for the BHL of 58tf while the Johson-Cook criterion resulted in a 1% error for the BHL of 130tf. Thus, in the case where the sheet metal is in a very restricted condition it becomes feasible to use the Johnson-Cook criterion.

Is very important to note that is more interesting to use a failure criterion with only one calibration constant, as the case of the Maximum Shear Stress (MSS) and the Oh et al. criteria. Such criteria were able to deliver a computational error of 3% for the BHL of 130tf and an average error of 7% for the BHL of 80tf. As the most striking contribution is worth to note that the two criteria mentioned above can be obtained by a simple uniaxial tensile test.

For the sheet metal community, the achieved results presented in this work can be used by choosing a specific failure criterion prior the tooling development to have a first approach of the process parameters

to be implemented prior the current production of new product. Also the failure criteria can be used to troubleshoot stamping issues based on strain analysis and sheet formability.

Declarations

a. Funding (information that explains whether and by whom the research was supported): The authors would like to thank CNPq Agency (Brazil) for the for the grant to Mr. Paulo Victor Prestes Marcondes.

b. Conflicts of interest/Competing interests: Not applicable.

c. Availability of data and material: Not applicable.

d. Code availability: Not applicable.

e. Ethics approval: Not applicable.

f. Consent to participate: Not applicable.

g. Consent for publication: The authors consent for the publication of the present work.

References

1. Keeler S e Menachem K. Advanced High-Strength Steels Application Guidelines. Worldautosteel, 2014.
2. Tepedino J. A. Aplicação de Curvas Limite de Conformação na previsão de rupturas em bordas de peças estampadas. 2014.
3. Bao, Y., and Wierzbicki T. On fracture locus in the equivalent strain and stress triaxility space.*Int J Mech Sci*, 2004: 46(1): 81-98.
4. Tomasz Wierzbicki, Yingbin Bao, Young-Woong Lee, Yuanli Bai. Calibration and evaluation of seven fracture models. *International Journal of Mechanical Sciences*, 2005: 47: 719–743.
5. Habibi N, Ramazani A e Prahl U. Failure predictions of DP600 steel sheets using various uncoupled fracture criteria. *Engineering Fracture Mechanics.* 2017. 1-15.
6. Dunand M e Mohr D. Determination of (multiaxial) ductile fracture properties of trip steel sheets using notched tensile specimens. Report 193. *Technical report, Impact and Crasworthiness Laboratory. MIT, Cambridge MA.*2000.
7. Tresca. Tresca Memoir on the flow of solid bodies under strong pressure.*Comptes-rendus de l'académie des sciences.* 1864. 59:754-8.
8. Johson GR e Cook WH. Fracture characteristics of three metals subjected to various strains, strain rates, temperatures and pressures. *Eng Fract Mech .*1985. 101: 36-44.
9. Lou Y, Huh H, Lim S e Pack K. New ductile fracture criterion for prediction of fracture forming limit diagrams of sheet metals.*Int J Solids Struct .*2012. 49:3605-15.

10. Oh S, Chen C e Kobayashi S. Ductile Fracture in axissymmetric extrusion and drawing - part 2: workability in extrusion and drawing. *J Eng Industry.* 1979. 101: 36-44.
11. Keunhwan Pack, Meng Luo, Tomasz Wierzbicki. Sandia Fracture Challenge: blind prediction and full calibration to enhance fracture predictability. *Int J Fract*, 2014: 186:155–175.
12. Chemin Filho R. A. Estudo da fratura de aços de nova geração DP600 através da variação de pressão no prensa-chapas. *Tese de Doutorado em Engenharia Mecânica pela Universidade Federal do Paraná*, 2011.
13. Abaqus V16.4/CAE - *User's Guide (*2014).
14. Bai Y e Wierzbicki T. Application of extended Mohr-Coulomb criterion to Ductlie Fracture. *Int J Fract.* 2010. 1-20.
15. Lajarin SF, Marcondes PVP, Dependence of plastic strain and microstructure on elastic modulus reduction in advanced high-strength steels, Journal of the Brazilian Society of Mechanical Sciences and Engineering, 2018. 40:87.
16. Lajarin S. F. Influência da variação do módulo de elasticidade na previsão computacional do retorno elástico em aços avançados de alta resistência. Tese de Doutorado em Engenharia Mecânica pela Universidade Federal do Paraná, 2012.

Figures

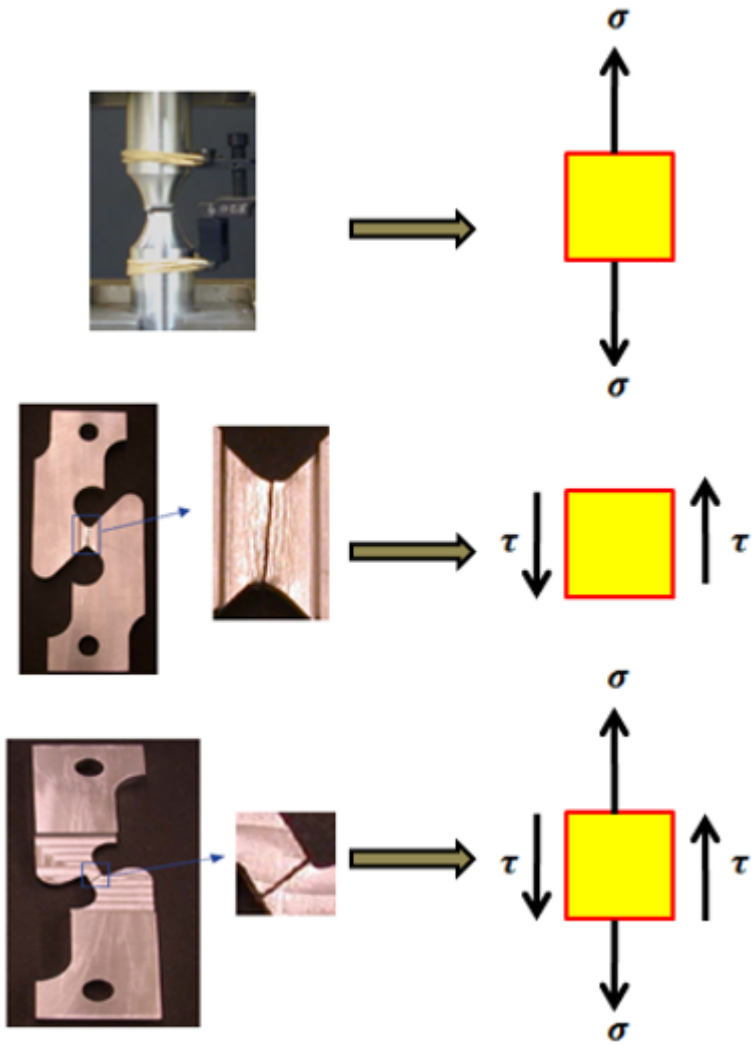

Figure 1

Specimens used by [3] to define the fracture envelope.

Figure 2

Drawing of the modified Nakazima tool used for tests and the computational model.

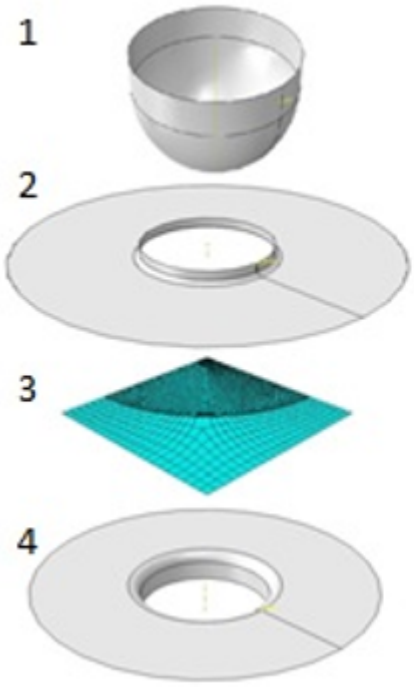

Sequence	Name	Format	Type
1	Punch	Shell	Rigid
2	Blank holder	Shell	Rigid
3	Sheet	Shell	Deformable
4	Die	Shell	Rigid

Figure 3

Computational model and its characteristics.

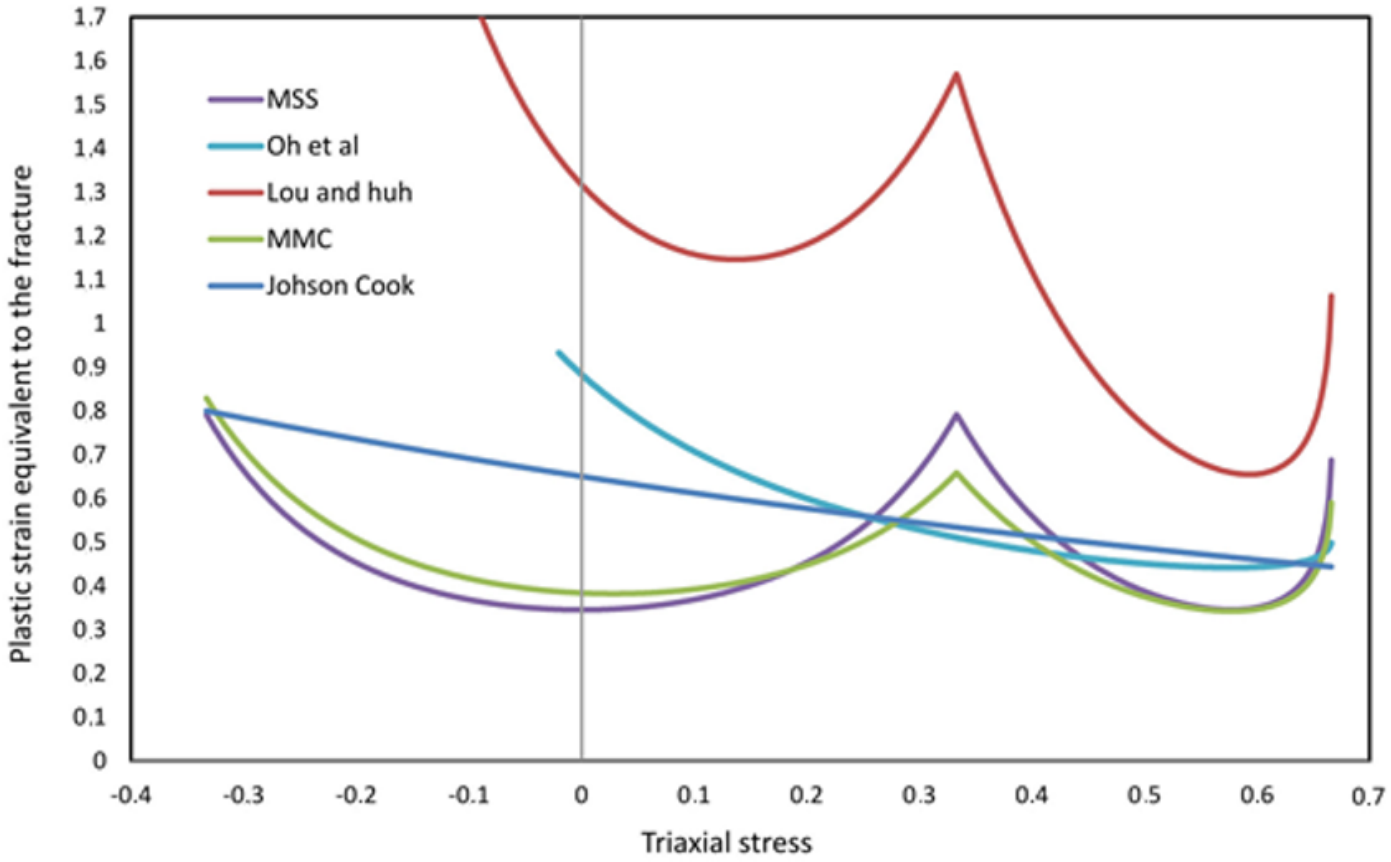

Figure 4

Fracture envelopes obtained with the constants determined by [5] for the DP600.

$\sigma_e(MPa)$	$\sigma_{LRST}(MPa)$	$\%AL$	$E\ (GPa)$	$A(MPa)$	n
387	605	23	207	1010	0.188

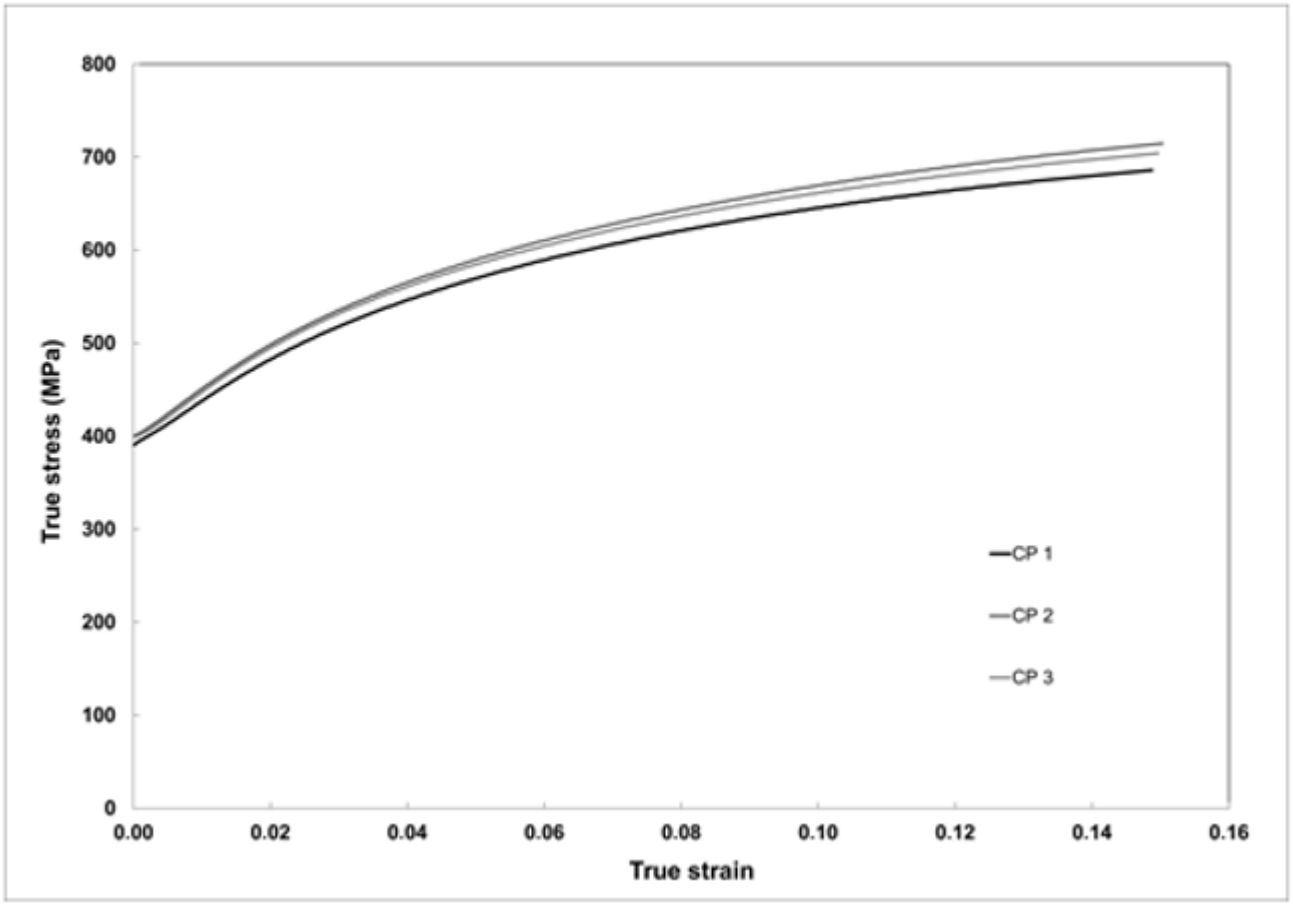

Figure 5

Fundamental mechanical properties and true stress vs true strain curve obtained by [15].

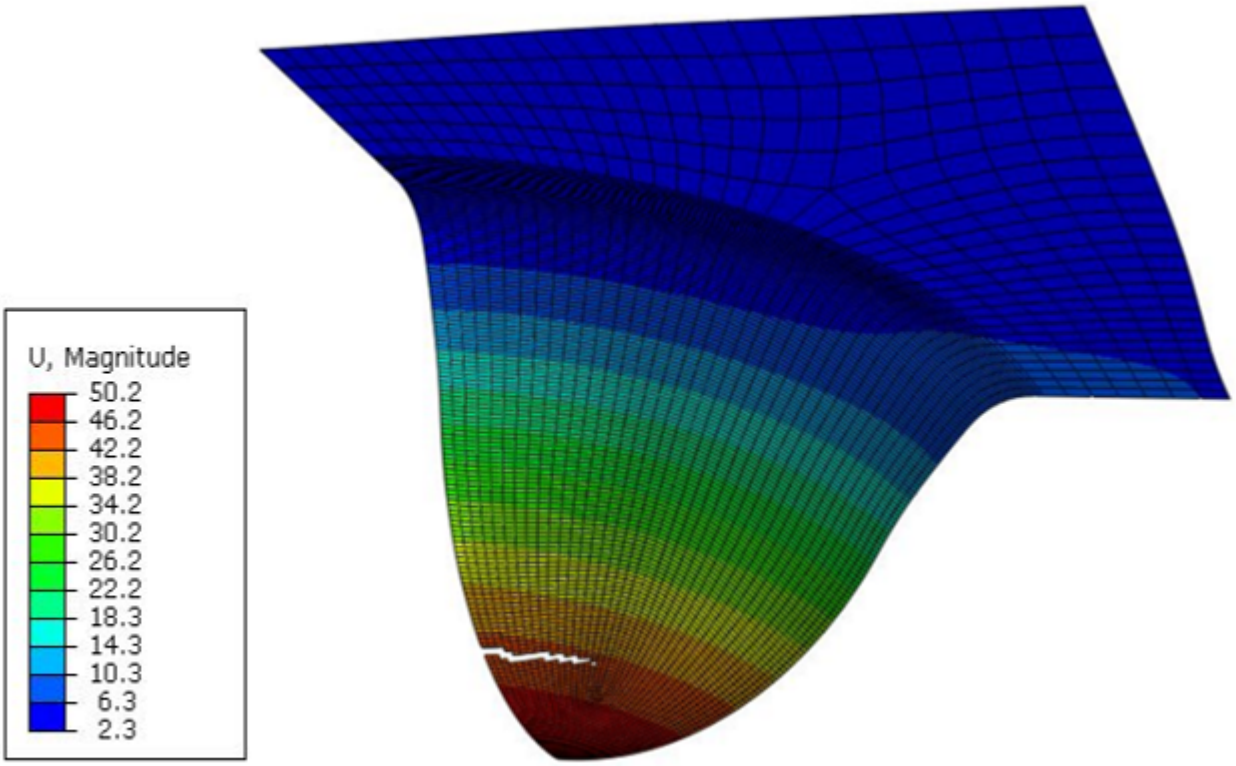

Figure 6

Crack initiation by failure criteria implemented in the computational model.

Figure 7

Errors obtained by computational models for a BHL of 58tf (a), 80tf (b) and 130tf (c).

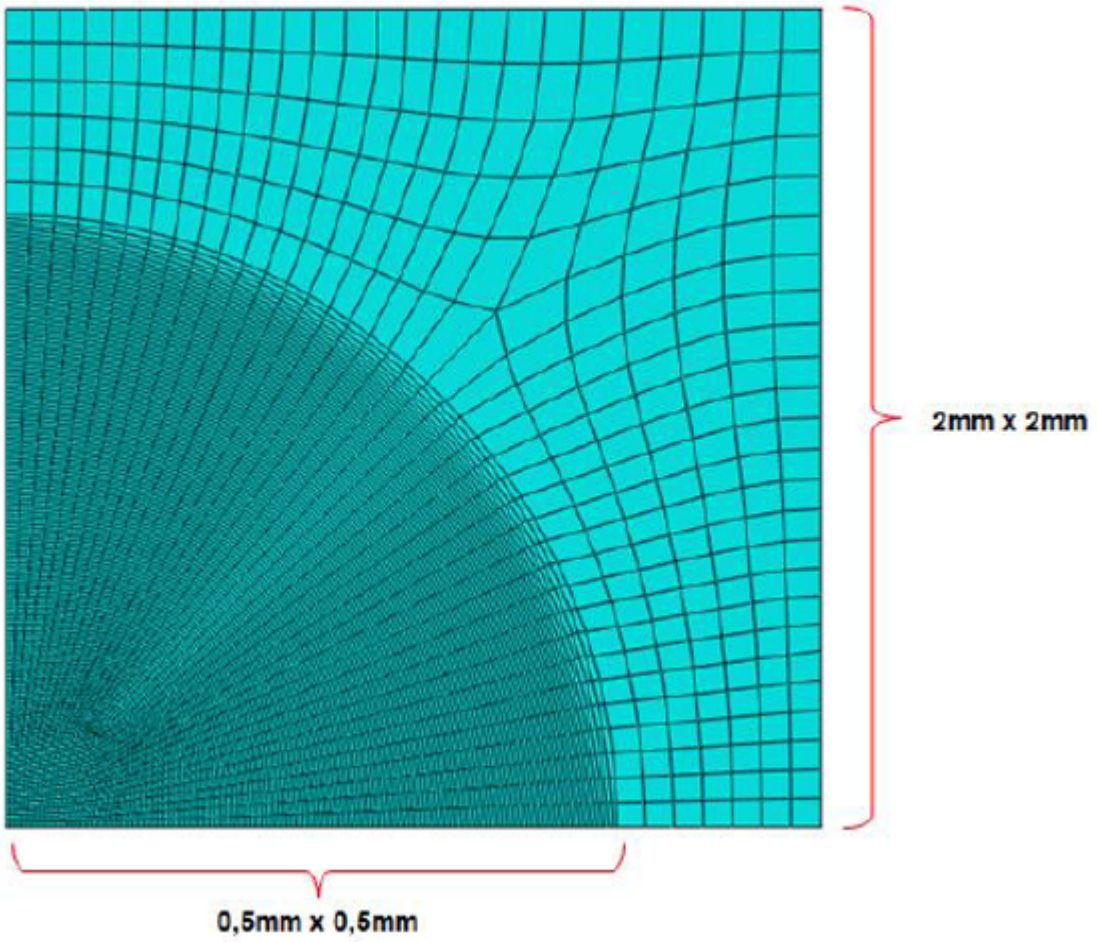

Figure 8

Meshing applied for all the simulations.

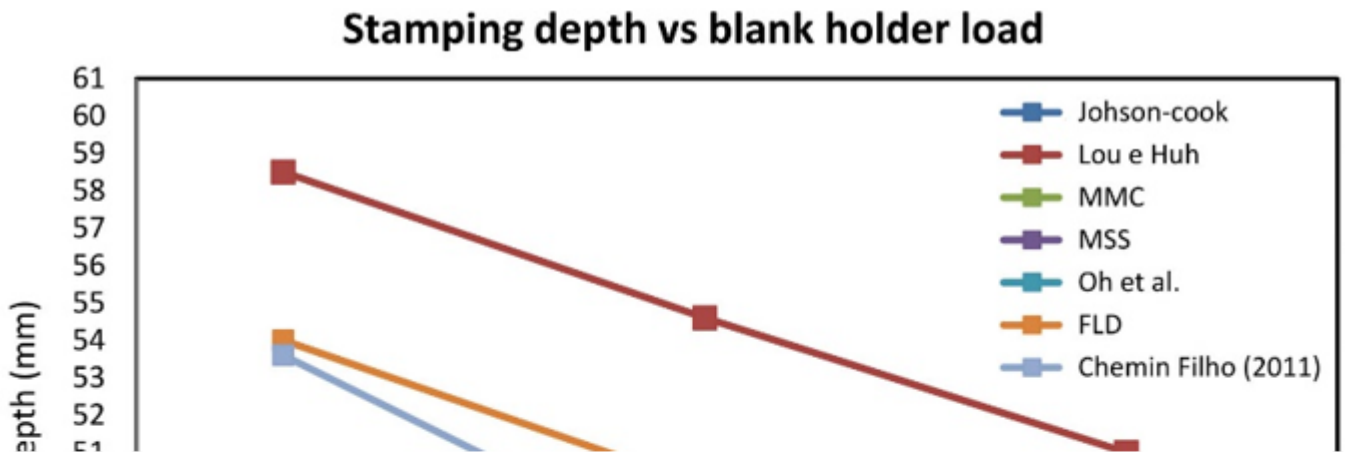

Figure 9

Comparison between the obtained results.